

Catalase-peroxidase KatG of *Burkholderia pseudomallei* at 1.7 Å resolution

Xavi Carpena¹, Suvit Loprasert², Skorn Mongkolsuk², Jacek Switala³
Peter C. Loewen^{3*} and Ignacio Fita¹

¹CID-CSIC, Jordi-Girona 18-26
08034 Barcelona, Spain

²Laboratory of Biotechnology
Chulabhorn Research Institute
Lak Si, Bangkok 10210
Thailand

³Department of Microbiology
University of Manitoba
Winnipeg, Man., Canada, R3T
2N2

The catalase-peroxidase encoded by *katG* of *Burkholderia pseudomallei* (BpKatG) is 65% identical with KatG of *Mycobacterium tuberculosis*, the enzyme responsible for the activation of isoniazid as an antibiotic. The structure of a complex of BpKatG with an unidentified ligand, has been solved and refined at 1.7 Å resolution using X-ray synchrotron data collected from crystals flash-cooled with liquid nitrogen. The crystallographic agreement factors *R* and *R*_{free} are 15.3% and 18.6%, respectively. The crystallized enzyme is a dimer with one modified heme group and one metal ion, likely sodium, per subunit. The modification on the heme group involves the covalent addition of two or three atoms, likely a perhydroxy group, to the secondary carbon atom of the vinyl group on ring I. The added group can form hydrogen bonds with two water molecules that are also in contact with the active-site residues Trp111 and His112, suggesting that the modification may have a catalytic role. The heme modification is in close proximity to an unusual covalent adduct among the side-chains of Trp111, Tyr238 and Met264. In addition, Trp111 appears to be oxidized on C^{δ1} of the indole ring. The main channel, providing access of substrate hydrogen peroxide to the heme, contains a region of unassigned electron density consistent with the binding of a pyridine nucleotide-like molecule. An interior cavity, containing the sodium ion and an additional region of unassigned density, is evident adjacent to the adduct and is accessible to the outside through a second funnel-shaped channel. A large cleft in the side of the subunit is evident and may be a potential substrate-binding site with a clear pathway for electron transfer to the active-site heme group through the adduct.

© 2003 Elsevier Science Ltd. All rights reserved

*Corresponding author

Keywords: crystal structure; catalase-peroxidase; KatG; isoniazid

Introduction

The bifunctional catalase-peroxidases are enzymes that degrade hydrogen peroxide either as a catalase ($2\text{H}_2\text{O}_2 \rightarrow 2\text{H}_2\text{O} + \text{O}_2$) or as a peroxidase ($\text{H}_2\text{O}_2 + 2\text{AH} \rightarrow 2\text{H}_2\text{O} + 2\text{A}$), thereby preventing cellular damage induced by breakdown products of H_2O_2 such as the highly reactive hydroxyl radical. The

catalytic reaction, with a more rapid turnover rate, dominates over the peroxidatic reaction, making the enzyme appear to be a catalase rather than a peroxidase, despite the close sequence resemblance to plant peroxidases.¹ This resemblance to plant peroxidases was clearly illustrated when the change of a tryptophan residue to phenylalanine in the catalase-peroxidase distal heme pocket reduced the catalytic activity by 1000 fold (of *Escherichia coli* HPI) and increased the peroxidatic activity by threefold.^{2–4} The crystal structure of the catalase-peroxidase from *Haloarcula marsimortui* has revealed a core structure very similar to that present in plant peroxidases.⁵

The catalase-peroxidases gained significant notoriety in 1992 when it was confirmed that mutation of *katG*, encoding the *Mycobacterium tuberculosis* KatG, imparted isoniazid (INH) resistance.⁶ The obvious importance of isoniazid

Abbreviations used: INH, isonicotinic acid hydrazide, C₆H₇N₃O (isoniazid); HMCP, *H. marismortui*; BpKatG, catalase-peroxidase from *B. pseudomallei*; EcKatG, catalase-peroxidase from *E. coli*; MtKatG, catalase-peroxidase from *M. tuberculosis*; CP, catalase-peroxidase; HRP, horseradish peroxidase; CCP, cytochrome c peroxidase; APX, ascorbate peroxidase.

E-mail address of the corresponding author:
peter_loewen@umanitoba.ca

Table 1. Data collection and structural refinement statistics and structure analysis

	BpKatG_NAT ^a	BpKatG_INH ^b
<i>A. Data collection statistics</i>		
Unit cell parameters		
<i>a</i> (Å)	100.9	100.9
<i>b</i> (Å)	115.1	115.6
<i>c</i> (Å)	175.3	175.2
Resolution range (Å)	20–1.80 (1.86–1.80)	18–1.70 (1.73–1.70)
Unique reflections (<i>F</i> > 0)	181,754 (17,651)	221,727 (11,076)
Completeness (%)	95.6 (93.8)	99.2 (99.9)
<i>R</i> _{sym} (%) ^c	5.3 (45)	7.3 (58)
<i>I</i> / <i>σ</i> (<i>I</i>)	14.7 (2.4)	13.5 (2.7)
Redundancy	3.3 (3.0)	3.6 (3.6)
<i>B. Refinement statistics</i>		
Resolution	20–1.80 (1.85–1.80)	18–1.70 (1.75–1.70)
Working set	162,436 (11,553)	199,550 (14,281)
Free reflections	17,971 (1321)	22,115 (1573)
<i>R</i> _{cryst} (%) ^d	14.7 (23.6)	15.3 (23.5)
<i>R</i> _{free} (%)	18.3 (26.5)	18.6 (26.7)
<i>C. Structure analysis</i>		
No. non-hydrogen atoms		
BpKatG (subunit A)	5543	5543
Main-chain	2863	2863
Side-chain	2680	2680
BpKatG (subunit B)	5531	5531
Main-chain	2861	2861
Side-chain	2670	2670
Water molecules	2044	2295
Hemes (sub. A,B)	86	86
Sodium ions	2	2
PEO	4	4
rmsd from ideality		
Bond lengths (Å)	0.017	0.013
Bond angles (deg.)	1.46	1.30
Averaged <i>B</i> factor (Å ²)		
Subunit A	16.9	16.9
Main-chain	15.2	15.4
Side-chain	18.7	18.6
Subunit B	16.5	16.5
Main-chain	14.6	14.9
Side-chain	18.4	18.2
Water molecules	26.1	28.7
Hemes (sub. A and B)	14.9	15.3
Sodium ions	25.7	21.4
PEO	35.5	34.0

^a Values in parentheses correspond to the highest-resolution shell.

^b The BpKatG_INH corresponds to crystals where 100 mM INH was added to the cryobuffer (see Materials and Methods); however, there is no significant change, with respect to the data obtained without INH. The structure obtained without soaking with INH, though at lower resolution, is used in the present analysis as a control.

^c $R_{\text{sym}} = \frac{\sum_{hkl} \sum_j |I_{hkl,j} - \langle I_{hkl} \rangle|}{\sum_{hkl} \langle I_{hkl} \rangle}$, where *j* extends to all the observed *hkl* symmetry-related reflections.

^d $R_{\text{cryst}} = \frac{\sum \|F_{\text{obs}}\| - |F_{\text{calc}}|}{\sum \|F_{\text{obs}}\|}$. *R*_{free} is as for *R*_{cryst} but calculated for a test set comprising reflections not used in the refinement

as an anti-tuberculosis drug and the prevalence of *katG*-induced INH-resistant *M. tuberculosis* strains causing tuberculosis led to great interest in determining the structure of a KatG with several groups

worldwide attempting to solve its structure. Unfortunately, attempts to crystallize a number of different catalase-peroxidases were without success until very recently, when the crystallization of the enzymes from *Haloarcula marismortui*,^{5,7} *Synochococcus*,⁸ and *Burkholderia pseudomallei*⁹ and of the C-terminal domain of *E. coli* HPI were reported.¹⁰ Curiously, despite many years of study the actual *in vivo* peroxidatic substrate of the catalase-peroxidases has not been identified. INH is not a normal bacterial metabolite, and its reaction must arise from interaction in a binding site intended for the natural substrate.

The large size of the catalase-peroxidase subunits, containing two distinct, sequence-related domains, relative to the plant peroxidases may have been the result of a gene duplication and fusion event.¹¹ The N-terminal domain contains the heme and active-site residues, that when modified affect enzyme activity. The C-terminal domain has less sequence similarity, and does not have the conserved heme active-site motif characteristic of peroxidases. The heme occupancy for many catalase-peroxidases appears to be partial, originally determined to be 0.5 heme per subunit.¹² The presence of a heterogeneous mixture of dimers and tetramers in *E. coli* HPI with zero, one and two, or one, two and three hemes was confirmed recently,² and this may have been a major problem in crystal formation. In fact, the catalase-peroxidases from *H. marismortui* (HMCP) and *B. pseudomallei* (BpKatG) were purified with an apparently higher heme to subunit ratio, and this less heterogeneous protein proved amenable to crystallization.

Here, we describe the structure solution and refinement at 1.7 Å resolution of BpKatG from improved crystals.⁹ The overall structure is very similar to that of the *H. marismortui* CP but with a number of important unreported features made possible by the higher-resolution data that provide exciting insights into the catalytic possibilities of the enzyme.

Results and Discussion

Overall description of the BpKatG structure

The electron density map defines main-chain and side-chain atoms of 1428 amino acid residues, two metal ions and two modified heme groups in two subunits and 2314 water molecules. The 34 N-terminal residues of both subunits do not appear in the structure, but the maps show clear continuity over the complete length from Asn35 to Ala748 in both subunits. Residue Asn35 is refined only about the main-chain atoms and the side-chain atoms are not included in the model. The model has crystallographic agreement *R* and *R*_{free} factors of 15.3 and 18.6% for 199,550 reflections in the resolution shell between 1.7 Å and 18.0 Å (Table 1). The average root-mean-square (r.m.s.) deviation after superimposition of the two subunits is 0.33 Å for

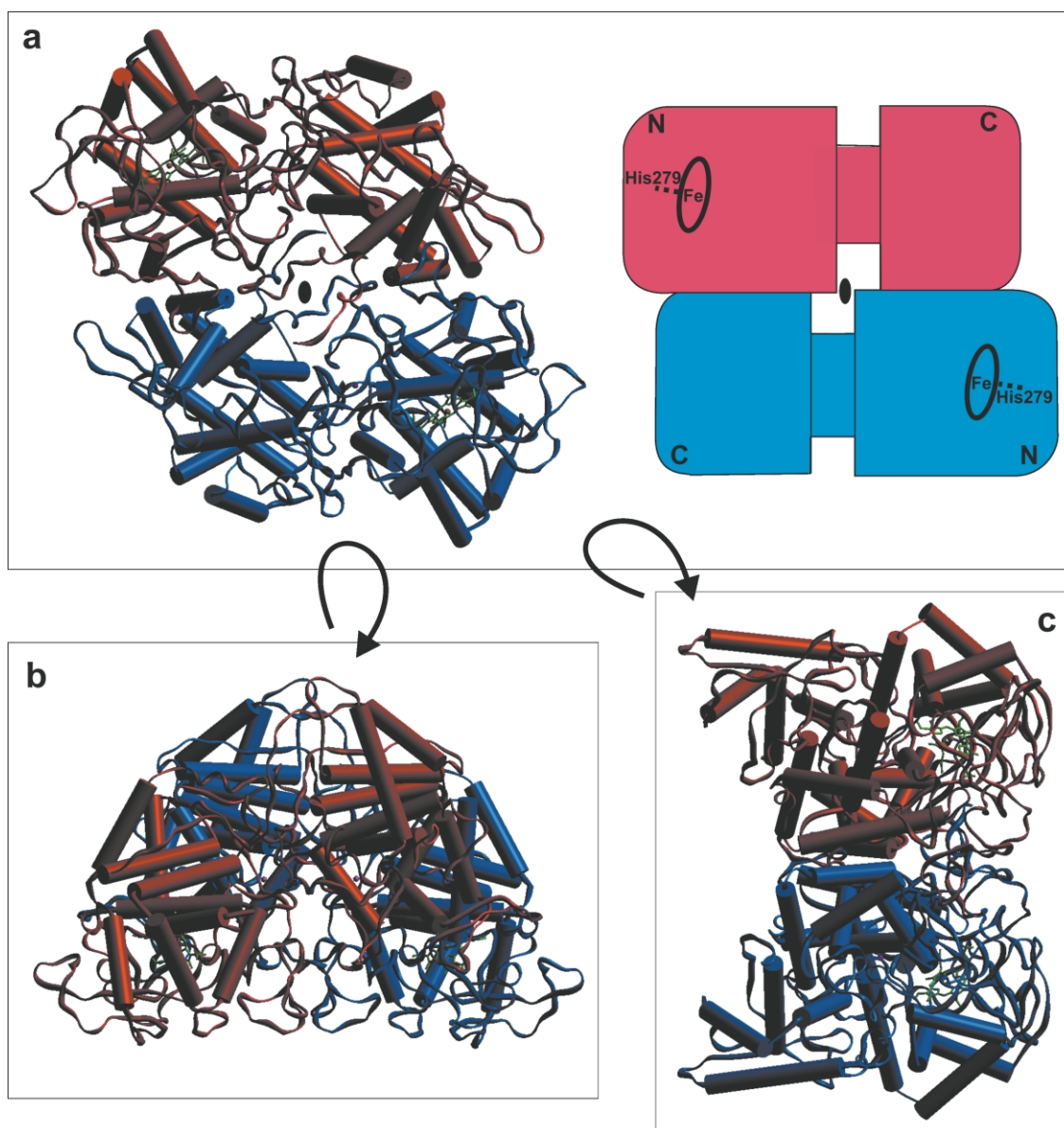


Figure 1. Three views of BpKatG rotated 90° relative to each other. The view in (a) is oriented looking down the axis of 2-fold symmetry (indicated by the oblong dot). The schematic on the right illustrates the relationship and interactions of the N and C-terminal domains in each subunit. (b) The molecule is rotated forward 90° so that the reader is viewing the molecule from the top in (a). (c) The molecule is rotated 90° to the right so that the reader is viewing the molecule from the left end in (a). The 20 helical regions are represented by tubes.

the 714 C^α atoms and 0.76 \AA for all atoms, indicating only minor differences between the two subunits. Also, a testament to the quality of the data was the clarity, in the electron density, of a number of errors in a 12 amino acid residue region of the predicted sequence. An insertion and a deletion error were subsequently identified in the DNA sequence, which was corrected in GenBank (accession number AY040244).

The two crystallographically independent protein subunits found in the BpKatG crystal structure are related by accurate non-crystallographic 2-fold symmetry (179.7° after superimposition of the two subunits). The axis is perpendicular to the

crystallographic c axis at 30° from the a axis. The dimer has a rather rectangular shape of about $85 \text{ \AA} \times 95 \text{ \AA} \times 105 \text{ \AA}$ in size with the dimer 2-fold axis oriented perpendicular to the largest face (Figure 1). In turn, individual subunits can be centered in parallelograms of about $45 \text{ \AA} \times 50 \text{ \AA} \times 95 \text{ \AA}$ with the two subunits in the dimer oriented anti-parallel to each other with a left-handed twist of about 30° . The two subunits in the dimer present extensive surface contacts of 7000 \AA^2 , but without any significant interdigitation. The subunit organization, with well defined globular N (to residue 438) and C-terminal regions arranged along the longest subunit axis, together with the anti-parallel

disposition of subunits in the dimer results in the intersubunit interactions being dominated by crossover interactions between the larger N-terminal domain of one subunit and the smaller C-terminal domain of the other, with a contact area of $2 \times 2450 \text{ \AA}^2$. However, interactions between N-terminal regions are present, with a contact area of $2 \times 1250 \text{ \AA}^2$ and could play a dominant role in dimerization.¹³ Residue Cys27, not visible in the electron density, has been shown to participate in a conserved disulfide bond between subunits in KatG of *M. tuberculosis*, although data indicate that this bond is not a prerequisite for the formation of dimeric KatG.¹³

The structure is similar in many respects to that of the *H. marismortui* catalase-peroxidase,⁵ to the extent that the average r.m.s. deviation for 685 C α atoms, after superimposition of the two subunits and elimination of 29 non-corresponding residues, is 1.05 Å. Consideration of just the 133 highly conserved residues in the ten α -helical regions of the N-terminal region of the sequence (to residue 426), revealed an r.m.s. deviation between HMCPx and BpKatG of just 0.43 Å. The relative disposition of the two globular domains of the subunits, the N and C-terminal domains, appears to be extremely well preserved, as expected from the large contact area between the two domains of about 3300 \AA^2 , which is difficult to reconcile with the concept of a flexible hinge joining the two domains.⁵

Ramachandran plots (not shown) confirm that all residues in both subunits fall within the energetically favorable regions,¹⁴ but a number of other unusual features were noted. Three *cis* proline residues (135, 228 and 509) are present, and six residues with double conformations (Ser50, His55, Thr119, Glu198, Arg426 and Gln711) were identified in both subunits. Extra density suggestive of modification, most likely the result of oxidation, was evident on the side-chains of Trp111, Trp139 and Met266, also in both subunits (see below). The unusual covalent adduct involving the side-chains of Trp111, Tyr238 and Met264, found in HMCP, was identified in BpKatG in close proximity to a modification on the heme (also see below). Finally, the single cysteine residue in the model of both subunits, Cys556, exhibited lower electron density than expected, which could be due to irradiation effects.^{15,16}

About one-third of the residues of BpKatG exist in 20 α -helical regions and a small amount of β -sheet, with the remainder existing in regions interspersed among the helical coils (Figure 1). The individual subunits are organized in two structurally related domains, identified originally on the basis of sequence similarity.¹¹ The N-terminal domain and the C-terminal domain of BpKatG can be superimposed on one another, revealing a striking conservation of α -helical segments with ten N-terminal helices coinciding with ten C-terminal helices (Figure 1). The r.m.s deviation of 133 C α atoms in the ten superimposed helical segments is 2.19 Å. This conserved motif of α -helical segments

is found in the more distantly related (approximately 25% sequence identity) family of plant peroxidases. For example, superimposition of the N-terminal segment of BpKatG onto cytochrome *c* peroxidase (CCP), ascorbate peroxidase (APX) (both class I peroxidases) and horseradish peroxidase (a class III peroxidase) revealed r.m.s. deviations of 0.97 Å, 1.22 Å and 2.03 Å, respectively, for the 133 C α atoms in the ten α -helical segments. In turn, superimposition of the C-terminal region of BpKatG onto the same proteins gave r.m.s. deviations of 3.62 Å, 3.75 Å and 4.06 Å, respectively. Clearly, demands on the heme-containing N-terminal domain of KatG have resulted in a greater conservation of structure relative to the peroxidases than in the hemeless C-terminal domain.

The heme environment is virtually identical with that in HMCP and similar to that of the plant peroxidases (Figure 2). On the distal side of the heme, the active-site triad of Arg108, Trp111 and His112 is typical of all catalase-peroxidases and of class I peroxidases such as yeast cytochrome *c* peroxidase and ascorbate peroxidase. In class 3 peroxidases, such as horseradish peroxidase, the Trp is replaced by a Phe, a change that greatly reduces catalytic activity in the catalase-peroxidases.²⁻⁴ On the proximal side, His279 is the fifth ligand to the heme iron atom as in the peroxidases, and it is in close association with the fully conserved Asp389, which interacts with the indole N atom from the proximal Trp330. Carbonyl oxygen atoms from residues 279 and 281, not participating in hydrogen bonds, are pointing towards the proximal Trp330 side-chain, with a shortest distance of 3.01 Å between the C β from Trp330 and the main-chain oxygen atom from residue 279. The same type of interaction is present in APX and in CCP, where it appears to be particularly strong. Comparison of other residues surrounding the heme group reveals greater similarity to CCP with decreasing similarity in APX and HRP. This might be taken to imply that the compound I radical of catalase-peroxidases will dissociate from the heme to a nearby amino acid side-chain, as happens in CCP. However, existence of a porphyrin cation radical has been demonstrated for both EcKatG² and MtKatG,¹⁷ indicating that a definition of the factors governing the migration of the radical remains elusive. The environment of the heme propionate groups is very similar between APX and BpKatG, with the only significant difference being the replacement of residue Arg172 in APX by Thr323 in BpKatG (Figure 3). Water molecule W4, the solvent molecule with the lowest temperature factor (5.1 \AA^2), presents a tetrahedral bonding geometry with hydrogen bonds to the carboxylate groups of the two heme propionate groups and to the essential distal residue Arg108 (Figure 2(a)). It is worth mentioning that main-chain oxygen atom from residue Lys283 is pointing towards the carbon atom in the carboxylate group of the propionate group on ring IV, at a distance of

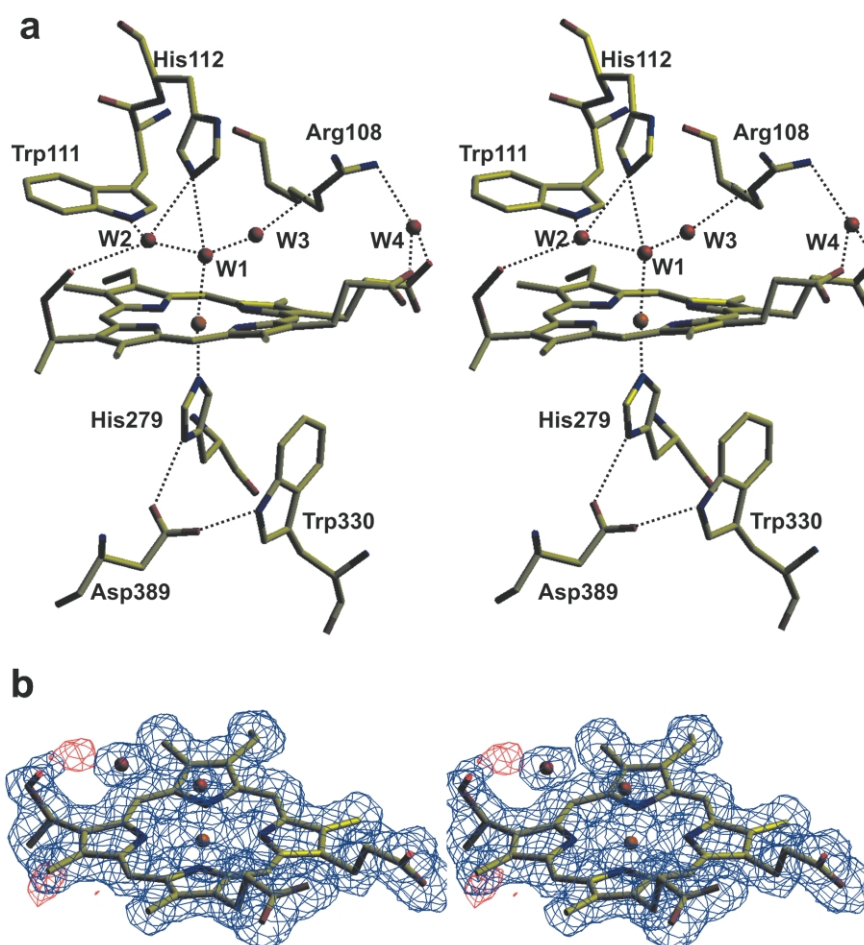


Figure 2. (a) Stereo view of residues in the vicinity of the heme. On the distal side, residues Arg108, Trp111 and His112 are shown, along with four water molecules labeled W1–W4. The adduct between Trp111 and Tyr238 is not shown here. On the proximal side, His279, Trp330 and Asp389 are shown. Interactions are indicated by the broken lines. (b) Stereo view of the $2F_o - F_c$ electron density map modeled at 1σ (in blue) and $F_o - F_c$ electron density map modeled at 3σ (in red) with the model of the heme superimposed. The postulated perhydroxy modification on the vinyl group of ring I is included.

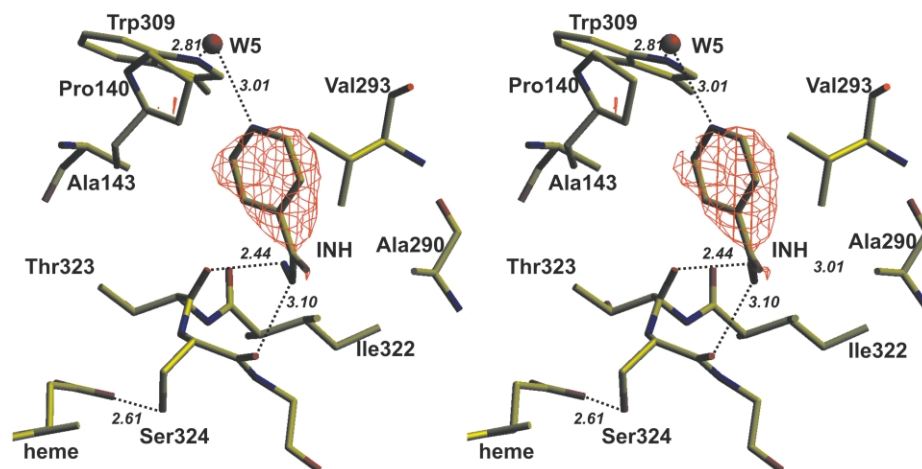


Figure 3. Stereo view of the environment surrounding the region of undefined electron density in the main channel leading to the heme. The $F_o - F_c$ electron density map modeled at 3σ is shown in red with a model of isoniazid (INH) superimposed. The individual nitrogen atoms of the $-NH-NH_2$ group of INH are shown interacting with the main-chain carbonyl oxygen atoms of Thr323 and Ser324. The side-chain $-OH$ of Ser324 is shown hydrogen bonded to the carbonyl oxygen atom of the heme propionate group. The ring nitrogen atom of INH is shown hydrogen bonding with water molecule W5, which also forms a hydrogen bond with the indole nitrogen atom of Trp309.

3.1 Å, making this an unlikely path for electron transfer.

Heme covalent modification

The electron density maps reveal an unambiguous addition of at least a two atom substituent to the vinyl group on ring I of the heme (Figure 2(b)). The nearby water molecule suggests that the modification can form hydrogen bonds, implying a polar nature. Hydrogen peroxide, as a substrate for the enzyme, has ready access to and will bind in the active site, making it a likely source for the modification *via* its addition across the vinyl group double bond. Including –OOH on the vinyl group in the model results in only a small amount of residual density in the $F_o - F_c$ map. The nature of such a modification satisfies the need for hydrogen bonding to the nearby water molecules and makes possible a facile removal or reversal of the modification. Indeed, it has not been possible to identify the modification by mass spectrometry, consistent with its expected labile nature, and only subtle changes in the 600–750 nm region of the absorption spectrum were evident.

The heme modification was not observed in HMCP, nor is it present in the closely related plant peroxidases. In all plant peroxidases, the residue equivalent to Tyr238 of BpKatG is a proline, and it is oriented to be in van der Waals contact with the vinyl group of ring I of the heme. This would sterically preclude modification of the heme on the vinyl group. A necessary prelude to the addition of –OOH to the heme of catalase-peroxidases would be exposure to hydrogen peroxide, and BpKatG was prepared from *E. coli* cells grown in aerated shake flasks for 22 hours, providing a long exposure to a highly oxygenated atmosphere and ample opportunity for the enzyme to encounter hydrogen peroxide. The highly oxidative environment experienced by BpKatG is further demonstrated by the oxidation of the C^{δ1} of the indole rings of Trp111 and Trp139. Excess density associated with this carbon atom was evident in the $F_o - F_c$ map, and oxidation of the indole ring at this location is not unexpected.¹⁸

The orientation of the –OOH substituent predicted in the model allows interaction with water molecule W2 in the heme distal pocket, thereby providing indirect contact with both the indole N atom of Trp111 and the imidazole ring of His112, two of the active-site residues required for reduction of compound I in the catalytic reaction. The orientation of the –OOH would allow its participation in catalysis, both during the formation of the Trp-Tyr adduct and in the reduction of compounds I and II, possibly helping to bind or orient the substrate hydrogen peroxide in conjunction with the indole NH group of Trp111. Involvement of the heme modification in the formation of compound I is less likely because of the greater distance to the side-chain of Arg108, which is required for the reaction.

Location of a metal ion

Unlike HMCP, which contained 16 chloride and six sodium or potassium ions, only one metal ion per subunit has been localized in the structure of BpKatG. Tentatively identified as sodium on the basis of its refinement properties and pentavalent, square pyramidal coordination structure with distances of about 2.35 Å (Figure 4). Surprisingly, this single cation is not related to any of the ions in HMCP, but is coordinated to the carbonyl oxygen atoms of residues 122, 124 and 494 as well as two water molecules. Water molecule W6 interacts with Glu128 and Glu198. Water molecule W7 interacts with the side-chain of Asp427 in which the carbonyl group is rotated about 60° relative to its orientation in HMCP. The cation and its counterion Asp427 side-chain are readily accessible to the exterior of the protein through a large, funnel-shaped channel that is unique to the catalase peroxidases (Figure 5). Along this channel there are a number of residues showing multiple conformations, in particular His55 and Glu198, further supporting the idea of an inlet or exit path for ions. The position of this putative sodium ion is about 7 Å from the corresponding positions in peanut, manganese or lignin peroxidases where a distal calcium ion had been reported.¹⁹ In barley peroxidase, replacement of the sodium ion by calcium appears related to the activation of the enzyme.²⁰

Trp111-Tyr238-Met264 adduct

The Trp111-Tyr238-Met264 adduct was first identified in the structure of HMCP and the electron density maps very clearly suggest its presence in BpKatG (Figure 6), supporting speculation that it may be a general feature of catalase peroxidases. The bond lengths determined in BpKatG of 1.69 Å between Cⁿ² of Trp111 and C^{ε1} of Tyr238, and 1.78 Å between C^{ε2} of Tyr238 and S^δ of Met264, are somewhat long in comparison to most covalent bonds. This apparent ambiguity about the nature of the bonds is reinforced by the evident intermediacy between sp² and sp³ character implied by the bond angles on the Tyr and Trp rings (Figure 6(b)). Despite this uncertainty, the existence of the adduct is supported by a recent matrix-assisted laser desorption/ionization time-of-flight mass spectrometry (MALDI-MS) analysis of tryptic peptides (data not shown), and by the existence of the Tyr-Trp structure in the antibiotics chlorpeptin and kistamicins.^{21,22} The mechanism leading to the formation of the adduct is fascinating to contemplate and a study of BpKatG variants should help to shed light on it.

The catalase-peroxidases bind hydrogen peroxide and use it as a substrate, providing a ready explanation for how the adduct might form. What is not as clear is whether the adduct has a function and provides some advantage to the enzyme. Other unusual adducts have been observed in

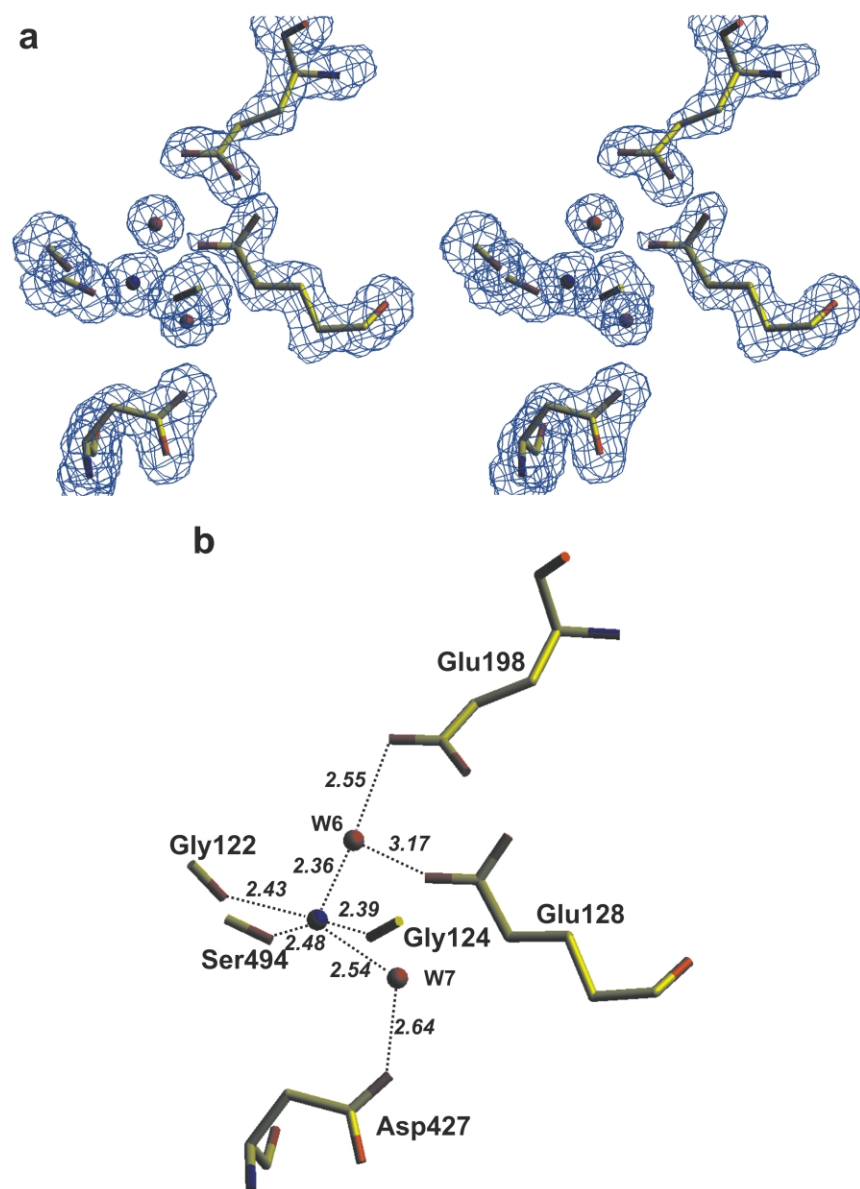


Figure 4. (a) Stereo view of the $2F_o - F_c$ electron density map modeled at 1σ in the vicinity of the metal ion with the model for the main-chain carbonyl groups of Gly122, Gly124 and Ser494, and water molecules W6 and W7 shown as coordinating groups. (b) Model of the residues in the environment of the metal ion with the interactions indicated by broken lines and associated distances between atoms indicated in italics.

peroxidases and in monofunctional catalases, including a hydroxy group on the C^β of Trp171 in lignin peroxidase,¹⁹ a methionine sulfoxide residue in the catalase from *Proteus mirabilis*,²³ an oxidized heme d in catalases from *E. coli* and *Penicillium vitale*,²⁴ and a covalent bond between the N^δ of His392 and C^β of Tyr415 of *E. coli* HPIL.²⁵ One rationale proposed for some of these modifications is that they stabilize the enzyme by reducing the likelihood of other, more damaging oxidations. The Trp-Tyr-Met adduct may impart a similar protection in that it will prevent further modification of the oxidation-susceptible methionine residue. The adduct may also contribute to the rigidity of what appears, from the clear definition of even surface-located side-chains, to be a very rigid enzyme, although the functional advantage of this is not clear. One other possibility is that it forms a route for electron transfer from the cleft region to the heme (see below).

A second catalytic center?

The side-chain of Arg426 exists in two orientations, of which the predominant (>70%) differs from the orientation in HMCP (Figure 7). Contributing to the complexity of this region are the two conformations of the side-chain of Thr119, of which the minor (<30%) is similar to the conformation in HMCP, suggesting coordination between the conformations of the two side-chains. Changes relative to HMCP (the single ion, the rotated Asp427 carbonyl group, and the displaced Thr119 and Arg426 side-chains) are in close proximity to one another, are associated directly or indirectly through hydrogen bonds or ionic interactions and represent the only changes in structure relative to HMCP in this region of the protein. This correlation suggests strongly that the changes are functionally related, and that the region of the protein may have an, as yet, undefined function, possibly

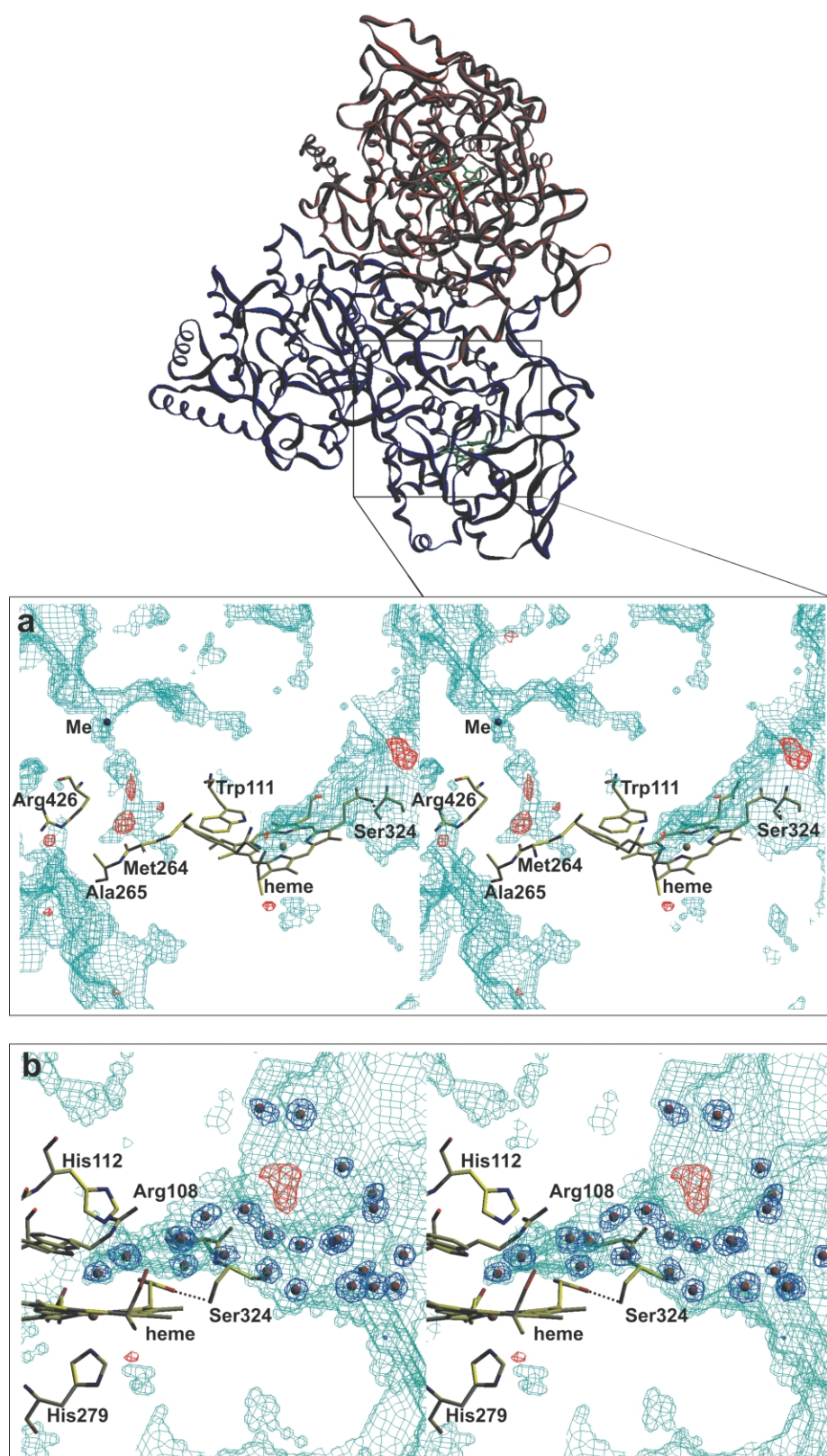


Figure 5. (a) Stereo view of the channel structure in the vicinity of the heme. The cross-section of the enzyme is oriented to include the main channel and region of undefined electron density ($F_o - F_c$ modeled at 3σ and shown in red), the modified heme, the Trp111-Tyr238-Met264 adduct, Arg426 adjacent to the large cleft, and the metal ion. The second funnel-shaped channel adjacent to the metal ion leads very close to the cavity created by the movement of Arg426. Some undefined electron density is visible in the $F_o - F_c$ map in this cavity. The region of the enzyme molecule that is included in (a) is indicated on the ribbon diagram of BpKatG shown at the top. The surface feature map generated by the program VOIDOO is presented in green. (b) Stereo view of the main channel leading to the heme. The

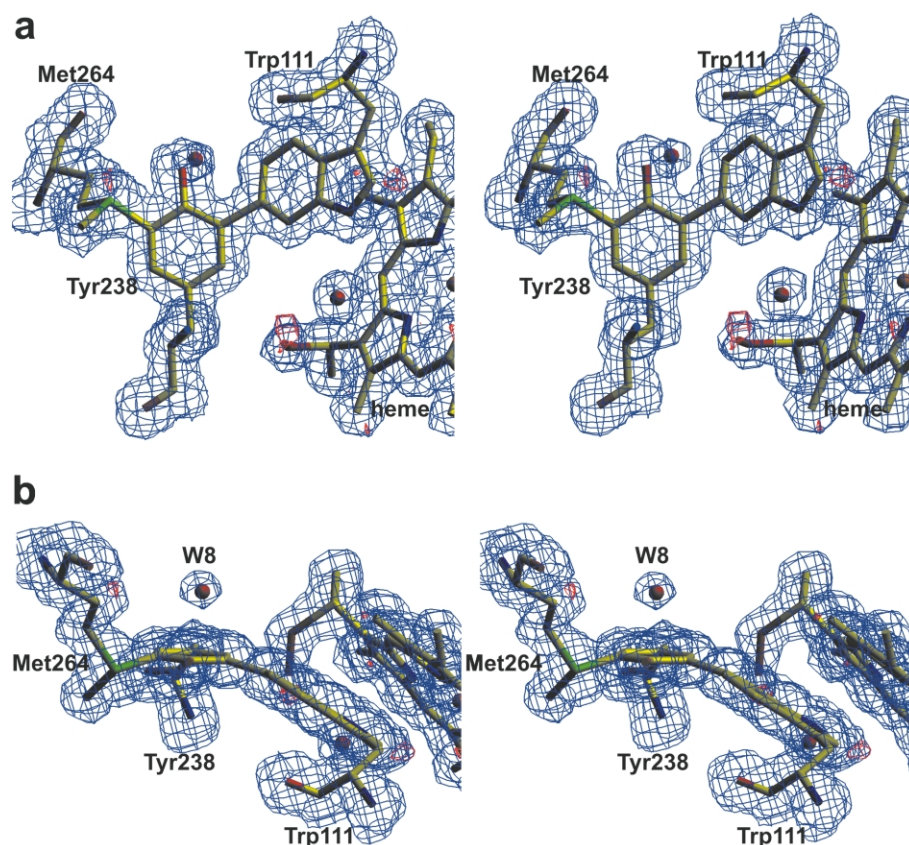


Figure 6. Two stereo views of the adduct formed among the side-chains of Trp111, Tyr238 and Met268. The $2F_o - F_c$ electron density map at 1σ is shown in blue and the model of the residues is superimposed. The view in (b) is rotated approximately 90° from that in (a), so that the reader is viewing the model towards the tyrosine ring OH. The intermediate sp^2 - sp^3 nature of the bonds of the adduct on the phenyl ring of Tyr238 is evident in the deviation from planarity of the substituents on the phenyl ring in (b). The $F_o - F_c$ electron density map at 3σ is shown in red. Note the extra density on Trp111.

as a second catalytic center besides the heme. This possibility is reinforced by the fact there is a region of undefined electron density located in the cavity vacated by the Arg426 side-chain in direct contact with the oxygen atom of the side-chain from Tyr238, the central residue of the covalent adduct.

Access channels and potential binding sites

Despite the apparent structural similarity to plant peroxidases, the larger subunit size of BpKatG (more than twice as large) results in the active site of BpKatG, including the resident heme, being buried more deeply within the subunit. The most obvious access route to the distal side of the heme, the active site of the enzyme for reaction with H_2O_2 , is provided by a channel positioned similarly to, but longer than, the access route in peroxidases. The channel in BpKatG has a pronounced funnel shape and is narrowest near residues Ser324 and Asp141, about 14 Å from the

heme iron atom (Figure 5). In peroxidases, the channel is not as constricted, and the peroxidatic substrate benzhydroxamic acid²⁶ binds to HRP in what is the equivalent of the constricted region of BpKatG closer to the heme. Substrate hydrogen peroxide entering the distal side cavity of BpKatG through the constricted portion of the channel would immediately come into contact with the active-site residues Arg109, Trp111 and His112 (Figure 5(b)) for generation of compound I in both the catalytic and peroxidatic modes of reaction, or for reduction of compound I in the catalytic reaction. Indeed, a continuum of water molecules is evident in this channel (Figure 5(b)). The mechanism by which organic substrates serve as electron donors for the peroxidatic reduction of compound I remains poorly defined.

Most peroxidases have a second access route, approximately in the plane of the heme, leading to the distal heme cavity, but the equivalent route in BpKatG is blocked by loops in the larger protein.

$2F_o - F_c$ electron density map of the water molecules in the channel (modeled at 1σ in blue) and the $F_o - F_c$ electron density map showing the region of undefined density (modeled at 3σ in red) are shown. The interaction between the side-chain of Ser324 and the heme propionate group is indicated by the broken line. The surface feature map indicated in green was generated in the program VOIDOO.

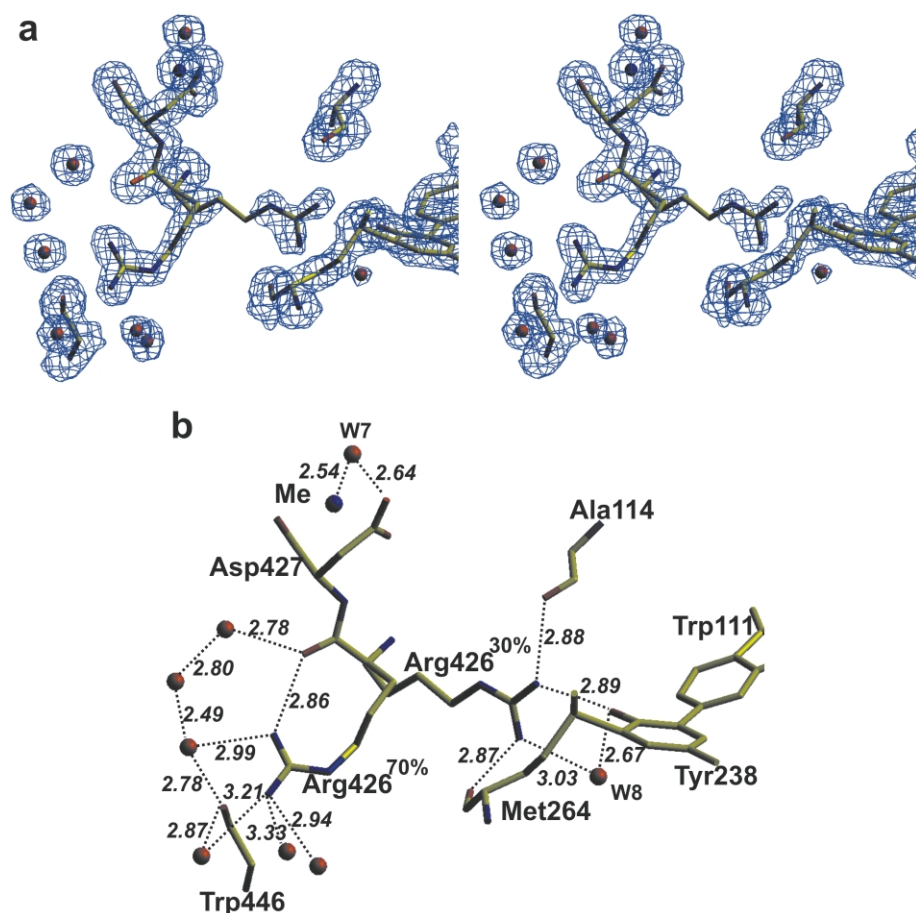


Figure 7. (a) Stereo view of the $2F_o - F_c$ electron density map modeled at 1σ in the vicinity of Arg426 with the model for both partial orientations of the Arg426 side-chain shown. The approximate proportions of the two orientations are indicated by the 30% and 70% designations. The main-chain atoms of Trp446 and other residues interacting with the Arg426 are included. (b) Model of the residues in the environment of Arg426 with the interactions indicated by broken lines and associated distances between atoms indicated in italics.

However, there does appear to be at least one other access channel providing direct access to the core of the protein in the vicinity of the single cation and to a region that encompasses two other structural features with possible functional significance. The first is a dramatic cleft in the side of the subunit formed between the two domains of the subunit that wraps around the protein. At one end of the cleft is located a well-defined, U-shaped region lined with polar residues (Figure 5(a)). Anionic residues, including the side-chains of Glu270, Asp587 and Glu589, and the carbonyl oxygen atoms of Ala262 and Ser265 surround a localized pocket of cationic groups including the side-chains of Lys422, Arg426 and Arg497. Significantly, the side-chains of Arg426 and Thr119 in their predominant conformations are located on the surface at the bottom of the U. They reduce the depth of the cleft slightly and allow the Arg426 side-chain to contribute to the cationic center on an otherwise predominantly anionic surface. Movement of the Arg426 side-chain to its minor conformation would increase the depth of the cleft and reduce the positively charged component on the surface. The associated rotation of the Thr119 side-chain

would change the hydrogen bonding environment of the cleft by moving the side-chain OH group to a more external location. Such a striking and well-defined cavity, combined with the potential for functional changes through the simple movement of two side-chains, begs the suggestion that this is the binding site for a substrate. Unfortunately, the identity of the *in vivo* peroxidatic substrate of BpKatG remains unknown, but, if the cleft is a binding site, its elongated nature may imply a substrate with an extended, possibly even polymeric character.

A necessary extension of this model is that if a substrate did bind at this site, it would be necessary to transfer electrons from it to the heme for the reduction of compound I or II, as part of the peroxidatic reaction. A relatively short path for such electron tunneling is immediately obvious, beginning with the main-chain carbonyl group of Ala265 on the surface of the cleft adjacent to Met264. As part of the Met264-Tyr238-Trp111 adduct, the MetS is most likely carrying a positive charge and would provide a draw for electrons from the cleft. In turn, the adduct provides a direct pathway for electron transfer to the heme. Analysis

Table 2. Explanation of the phenotype of some mutations in KatG of *M. tuberculosis* on the basis of their location in the BpKatG structure

Mutation	Peroxidatic activity ^a	Residue	Effect of mutation in BpKatG
<i>A. Category 1: mutations affecting the INH reaction specifically</i>			
Ser315Thr	0.6	Ser324	Either the hydrogen bond with the propionate group of the heme is broken or significant distortion in the side-chain is required to maintain hydrogen bonding and this would change the binding site for the hydrazine group of INH.
<i>B. Category 2: mutations affecting peroxidatic activity generally</i>			
Asn138Ser	0.1	Asn142	Binds to imidazole group of active-site His112 and change may distort spatial organization of active-site residues.
Leu148Arg	0.1	Leu152	Introduction of charged guanidinium group into a polar region would require significant distortion of the main chain of the protein.
His270Gln	0.1	His279	The proximal side fifth ligand of the heme iron is removed, reducing heme binding
Thr275Pro	0.3	Thr284	Significant distortion in the main chain of the protein on the proximal side of the heme would be required to accommodate the change.
Trp321Gly	0.3	Trp330	The indole ring is in close proximity to the proximal side His and removal may result in distortion of the main-chain atoms reducing heme binding and activity.
Asp381Gly	0.0	Asp389	The aspartate side-chain interacts with the proximal side fifth ligand of the heme and its removal causes disruption in heme binding.
<i>C. Group 3: mutations with an uncertain mechanism</i>			
Leu587Pro	ND ^b	Leu594	The location is on the surface but far removed from the active site or INH binding site. Protein folding or stability may be affected

^a Selected MtKatG variants and their peroxidatic activities taken from Rouse *et al.*²⁹

^b ND-not determined.

of the cleft may eventually provide insight into the *in vivo* substrate for KatG proteins.

In its minor conformation, the Arg426 side-chain is associated with the phenolic group on Tyr238 (Figure 7), similar to the predominant situation in

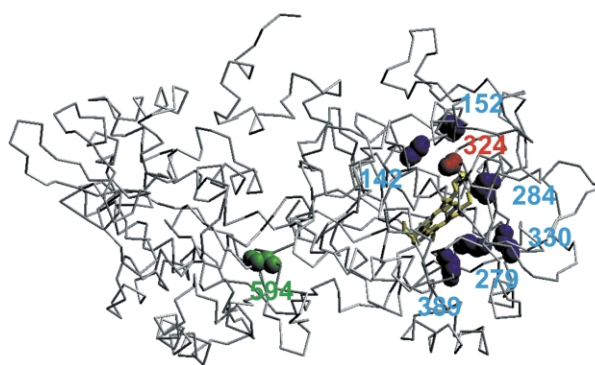


Figure 8. Location of mutations described in Table 2 located on a single subunit of BpKatG presented in the same orientation as the lower subunit shown in Figure 1(a). Only the main-chain atoms of the residues are shown and are represented as spheres. The residue in category 1 is colored red; the residues in category 2 are colored blue; and the residue in category 3 is colored green.

HmCP, where the Arg409 side-chain is associated with Tyr218. The cavity created by the movement of the side-chain to its predominant (>70%) conformation is located very close to the cleft region, and the slight movement of one or two side-chains would provide access from the cleft to the cavity. Perhaps more importantly, the other end of the cavity approaches the cation, which has direct access to the exterior through the second funnel-shaped channel (Figure 5(a)). A region of electron density that cannot be explained by partial occupancy of the Arg426 side-chain is present in the cavity, suggesting the presence of another bound molecule. It is not clear if this is an alternate substrate-binding site, but the cavity would provide easy access for hydrogen peroxide needed for the oxidation of Met264 in the formation of the covalent linkage.

Analysis of the potential isoniazid binding site

A region of undefined electron density is located just before the constricted region in the main channel leading to the distal heme cavity of BpKatG (Figures 3 and 5). The location of the density is over 10 Å further away from the heme than is the benzhydroxamic acid bound in HRP, but is in close proximity to Ser324, the equivalent of Ser315 in MtKatG, which is thought to be involved in INH binding because changing it interferes with INH activation. This extra density was found both in the structure obtained after a short soaking with INH and in the structure obtained without soaking (Table 1). However, no INH had been introduced to the enzyme subsequent to purification, and only phosphate buffer was used during the purification, making exposure to other pyridine-like molecules unlikely. Therefore, it is concluded that the undefined density is the result of a metabolic constituent of *E. coli*, that may closely resemble INH. One such molecule is pyridoxol

or vitamin B6, a common growth-medium component, and its oxidation would lead to pyridoxal required for the synthesis of pyridoxal phosphate. Another closely related common metabolite is nicotinamide, although why it would require oxidation is not clear. The potential for involvement in modification of common metabolites provides a role for the catalase-peroxidases other than being simply protective enzymes removing hydrogen peroxide. More importantly, it provides an explanation for why the enzyme has a binding site for isoniazid, which is not a normal bacterial metabolite.

Definition of the binding of isoniazid is one of the main goals of elucidating the structure of KatG and, despite the distance from the heme, the region around Ser324 is a strong candidate for INH binding. To investigate this possibility further, models of INH and pyridoxol were superimposed into the region of undefined density, and the environment was analyzed for the likelihood of their binding (Figure 3). The surrounding region is composed predominantly of hydrophobic amino acid residues including Pro140, Ala143, Ala290, Val293, Trp309 and Ile322, all of which might interact with the region of density suggesting the presence of a relatively hydrophobic molecule. Only two potential ionic or hydrogen bonding opportunities are presented at opposite ends of the electron-dense region. The hydrogen bond of indole N of Trp309 with water molecule W5 could potentially interact with the N atom of the pyridine ring of INH, pyridoxol or nicotinamide. At the opposite end, the carbonyl oxygen atoms of Thr323 and Ser324 are situated such that an interaction with the hydrazine portion of INH is possible. The oxidizable $-\text{CH}_2\text{OH}$ of pyridoxol would be oriented in close proximity to the same carbonyl oxygen atoms. The interaction of the nicotinamide $-\text{NH}_2$ group with the carbonyl group of Ile322 is predicted but the center to be oxidized is not evident, unless it is a very unusual reduced form of the ring.

The region in the main channel leading to the heme therefore presents a remarkably good candidate site for the binding of both INH and related pyridine derivatives. A possible mechanism for the oxidation of INH might involve distortion in the N-CO of INH bond caused by interaction with the Thr323-Ser324 carbonyl oxygen atoms. The side-chain of Ser324 forms a hydrogen bond with the carboxylate group of the heme propionate side-chain, and this direct association will result in a pull of electrons away from the serine residue towards the electron-deficient heme of compound I and compound II. This will result in polarization of the N-CO bond of INH, most likely leading to formation of the pyridine carbonyl and hydrazine radicals.²⁷ The pyridine carbonyl radical would be stabilized through resonance across the aromatic ring and delocalization of electrons from the pyridine nitrogen would break the hydrogen bond with water molecule W5, which might be necessary to allow reorientation of the molecule for

further reaction with NADH to form the InhA inhibitor.²⁸ The hydrazine radical might have an electron stripped for passage to the heme, generating a positively charged NH_2-NH^+ , which in turn would react rapidly with water to form NH_2-NHOH . Speculatively, if a molecule such as pyridoxol is the substrate, it might bind, oriented similarly to what has been proposed for INH, resulting in the $-\text{CH}_2\text{OH}$ *para* to the ring nitrogen atom being in close contact with the carbonyl oxygen atom of Thr322 ready for oxidation. As for INH, the electron-deficient heme of compounds I and II would serve to polarize electrons to promote the oxidation. Because Mn^{2+} was not introduced into the system and because KatG can activate INH independent of added Mn ion,²⁸ the role of Mn in this mechanism is not considered here.

This model provides an insight into the possible multiple roles of Ser315 of MtKatG in the oxidation of INH, and explains how its change to Thr would prevent reaction with INH. The first role lies in the main-chain interaction with the hydrazine portion of INH and direct participation in the catalytic reaction. The second role lies in providing a direct route for electron transfer from the INH to the radical of either compound I or compound II on the heme ring. Changing Ser to Thr would result in unfavorable interactions between the Thr side-chain and the heme propionate group in all conformers except one that could not form hydrogen bonds, thereby breaking the electron conduit. The other alternative of main-chain atom movement to allow hydrogen bonding would distort the catalytic site, preventing reaction.

All other residues in the pocket surrounding the INH-like electron density are fully conserved between BpKatG and MtKatG. Significantly, HMCP and the other catalase-peroxidases of haloarchaeobacterial origin have a one residue insertion of Asp269 compared to BpKatG, located in a loop adjacent to the pocket. The insertion forces the ring of the adjacent Pro270 into a position that would interfere with the region of INH-like electron density. The implication is that HMCP should not bind INH in this region, and this might explain why a similar region of electron density was not observed in the HMCP electron density maps.

On the basis of the structure of BpKatG, the mechanisms by which the various clinically identified mutations in MtKatG^{1,29} may impart INH resistance can be divided into three categories (Table 2). The first category includes only the Ser315Thr variant (equivalent to Ser324 in BpKatG), which has a minor effect on peroxidatic activity but a significant effect on INH activation, suggesting that INH binding and/or transfer of electrons to the heme is affected. The second category includes six variants with reduced peroxidatic activities, and correspondingly reduced abilities to activate INH. Included are Asn138Ser, Leu148Arg, His270Gln, His275Pro, Trp321Gly and Asp381Gly (equivalent to Asn142, Leu152, His279, His284, Trp330 and Asp389, respectively, in

BpKatG). The third category contains only one variant, Leu587Pro (equivalent to Leu594), which seems to be impart INH-resistance through enzyme instability, most likely the result of defective folding. Other clinical isolates of MtKatG, initially thought to impart INH resistance, including Ser140Asn, Ala350Thr, Arg463Leu and Leu587-Met are not included in the Table, because the variants retain native peroxidatic activities and native abilities to activate INH.^{1,29} Also not included in the list are the active-site variants Arg104Leu and His108Gln, which directly modify catalytic residues. The locations of the residues in BpKatG equivalent to the residues included in Table 2 are shown in Figure 8. The single residue in the first category (colored red) is found in the channel leading to the heme; the six residues in the second category (colored blue) are found in the general vicinity of the heme; and the single residue in the third category (colored green) is in the C-terminal domain.

These comparisons are based on the presumption of extensive similarity between the *M. tuberculosis* and *B. pseudomallei* enzymes and, indeed, the two enzymes are very similar. The sequences are 64.6% identical over the complete sequence of 749 residues, and, more importantly, they are 75.7% identical over 272 residues (residues 88–359) in the catalytic core of the enzyme. The discussions are also based on the assumption that BpKatG utilizes isoniazid as a substrate, and radical generation by BpKatG is indeed at a rate equivalent to that of *E. coli* HPI, about one-fifth of that of MtKatG³⁰ (data not shown).

The design of derivatives of INH that would be more effective and might possibly curtail the developing widespread resistance to INH in different strains of *M. tuberculosis* was one hoped-for objective that would result from the definition of the structure of KatG. Unfortunately, the structure suggests that such a goal will be elusive. The variability in the INH-resistance phenotypes is a result of mutations spread widely throughout the enzyme with no single focus or mechanism. Furthermore, the structural environment of the potential INH-binding site does not present obvious motifs that might be exploited for the binding of INH derivatives. The binding site is composed largely of hydrophobic residues surrounding a relatively small volume that is apparently optimized for a pyridine ring with a limited number of substituents, including the carbonyl hydrazide group *para* to the pyridine nitrogen (Figure 3(b)). One note of optimism is the fact that other different pyridine derivatives seem to bind to the site.

Conclusions

The crystal structure of the catalase-peroxidase of *B. pseudomallei*, determined at 1.7 Å resolution, presents a number of structural features that can be interpreted as implying the existence of, as yet

undetermined, catalytic functions of the catalase-peroxidases. The immediate environment of the heme-containing active site is structurally similar to that of plant peroxidases and to the catalase-peroxidase from *H. marismortui*, confirming its already ascribed functions as a catalase and a peroxidase. Indeed, the potential binding site for isoniazid is found within what is considered to be the usual substrate access channel of peroxidases. Despite its binding to catalase-peroxidases and the interest this has generated, isoniazid is not a normal substrate for the enzyme, but analysis of its binding site, a small hydrophobic pocket with limited functional capability, suggests that the natural substrate cannot be too different in size or shape.

The presence of a modification on the heme, likely a perhydroxylation, of a single sodium ion in each subunit, of multiple conformations of side-chains and of a new access channel to a cavity in the subunit interior, all within the same region of the subunit, imply the existence of a second, functionally important part of the enzyme. Immediately adjacent to this region are a large cleft on the enzyme surface, suggestive of a binding site for an extended substrate, and the unusual adduct of the side-chains of Trp111, Tyr238 and Met264, presenting a possible route for electron tunneling to the heme from substrates bound either in the cavity or in the cleft on the surface. Further work is required to define the actual *in vivo* peroxidatic substrates of the catalase-peroxidases, and the structure of BpKatG will provide direction to that study.

Materials and Methods

Crystallization and structure determination

The BpKatG protein analyzed in this work was purified from the catalase-deficient *E. coli* strain UM262 as described.⁹ Crystals were obtained at 20 °C by the vapor-diffusion, hanging-drop method with 2 µl of a 22 mg/ml of protein solution and 1 µl of the reservoir solution containing 16–20% (w/v) polyethylene glycol (PEG 4K), 20% (v/v) 2-methyl-2,4-pentanediol (MPD) and 0.1 M sodium citrate pH 5.6.⁹ Diffraction data were obtained from crystals cooled with a nitrogen cryostream using the same reservoir solution as cryobuffer at 20% PEG-4K. However, the best data set was obtained from a crystal where 100 mM INH had been added to the cryobuffer (Table 1). Crystals were primitive orthorhombic space group $P2_12_12_1$, with one dimeric molecule in the crystal asymmetric unit. The diffraction data set was processed using the program DENZO and scaled with program SCALEPACK.³¹ A part (10%) of the measured reflections in every data set were reserved for R_{free} monitoring during automatic refinement (Table 1). All the structural analysis reported in this work, except where indicated explicitly, has been done on the structure derived from the crystals soaked briefly with INH. However, no significant differences have been found with respect to the structure obtained without being exposed to INH. Even the extra density found in the major channel leading to the heme is found in both structures. Therefore, the structure derived from the crystal

after a short soak in INH is considered to be the native BKG structure. Reference to the unsoaked data set has been added only as a control to the presence of INH.

Structure determination was carried out with the program AMoRe³² and the CPx of *H. marismortui*⁵ as searching model. Phases were improved and extended to 1.7 Å resolution with the program ARP-WARP.³³ The resulting map showed clear continuity over the complete length of BpKatG from Asn35 to Ala748 in both subunits. The quality of the data was confirmed by the clarity in the electron density of a number of errors in a 12 amino acid residue region of the predicted sequence. Refinement was started with programs in the CNS suite³⁴ and completed using the program REFMAC³⁵ with solvent molecules modeled with the program WATPEAK³⁶ and manually with the graphics program O.³⁷ Solvent molecules were introduced only when they corresponded to the strongest peaks in the difference Fourier maps that could make at least one hydrogen bond with atoms already in the model. In the final rounds of refinement, the two subunits were treated independently with the bulk solvent correction applied and the whole resolution range available used for each variant (Table 1). The analysis of solvent accessibility and molecular cavities was carried out with program VOIDOO³⁸ using a reduced atomic radius for polar atoms in accounting for possible hydrogen bonds.³⁹ All the Figures were prepared using SETOR.⁴⁰

Protein Data Bank accession number

Structure factors and coordinates have been submitted to the Protein Data Bank under accession number 1MWV.

Acknowledgements

This work was supported by grants from DGICYT (BIO099-0865 and BIO2002-04419) to I.F., and OGP9600 from the Natural Sciences and Engineering Research Council of Canada (NSERC) to P.C.L. Many thanks are due to R. Perez and R. Eritja for their help in the experimental work.

References

- Heym, B., Alzari, P. M. & Honoré, N. and Cole, S. T. (1995). Missense mutations in the catalase-peroxidase gene, *katG* are associated with isoniazid resistance in *Mycobacterium tuberculosis*. *Mol. Microbiol.* **15**, 235–245.
- Hillar, A., Peters, B., Pauls, R., Loboda, A., Zhang, H., Mauk, A. G. & Loewen, P. C. (2000). Modulation of the activities of catalase-peroxidase HPI of *Escherichia coli* by site directed mutagenesis. *Biochemistry*, **39**, 5868–5875.
- Regelsberger, G., Jakopitsch, C., Ruker, F., Krois, D., Peschek, G. A. & Obinger, C. (2000). Effect of distal cavity mutations on the formation of compound I in catalase-peroxidases. *J. Biol. Chem.* **275**, 22854–22861.
- Regelsberger, G., Jakopitsch, C., Furtmuller, P. G., Rueker, F., Switala, J., Loewen, P. C. & Obinger, C. (2001). The role of distal tryptophan in the bifunctional activity of catalase-peroxidases. *Biochem. Soc. Trans.* **29**, 99–105.
- Yamada, Y., Fujiwara, T., Sato, T., Igarashi, N. & Tanaka, N. (2002). The 2.0 Å crystal structure of catalase-peroxidase from *Haloarcula marismortui*. *Nature Struct. Biol.* **9**, 691–695.
- Zhang, Y., Heym, B., Allen, B., Young, D. & Cole, S. (1992). The catalase-peroxidase gene and isoniazid resistance of *Mycobacterium tuberculosis*. *Nature*, **358**, 591–593.
- Yamada, Y., Saijo, S., Sato, T., Igarashi, N., Usui, H., Fujiwara, T. & Tanaka, N. (2001). Crystallization and preliminary X-ray analysis of catalase-peroxidase from the halophilic archaeon *Haloarcula marismortui*. *Acta Crystallog. sect. D*, **57**, 1157–1158.
- Wada, K., Tada, T., Nakamura, Y., Kinoshita, T., Tamoi, M., Sigeoka, S. & Nishimura, K. (2002). Crystallization and preliminary X-ray diffraction studies of catalase-peroxidase from *Synechococcus* PCC7492. *Acta Crystallog. sect. D*, **58**, 157–159.
- Carpena, X., Switala, J., Loprasert, S., Mongkolsuk, S., Fita, I. & Loewen, P. C. (2002). Crystallization and preliminary X-ray analysis of the catalase-peroxidase KatG from *Burkholderia pseudomallei*. *Acta Crystallog. sect. D*, **58**, 2184–2186.
- Carpena, X., Guarne, A., Ferrer, J. C., Alzari, P. M., Fita, I. & Loewen, P. C. (2002). Crystallization and preliminary X-ray analysis of the hydroperoxidase I C-terminal domain from *Escherichia coli*. *Acta Crystallog. sect. D*, **58**, 853–855.
- Welinder, K. G. (1991). Bacterial catalase-peroxidases are gene duplicated members of the plant peroxidase superfamily. *Biochim. Biophys. Acta*, **1080**, 215–220.
- Claiborne, A. & Fridovich, I. (1979). Purification of the *o*-dianisidine peroxidase from *Escherichia coli* B. Physicochemical characterization and analysis of its dual catalytic and peroxidatic activities. *J. Biol. Chem.* **254**, 4245–4252.
- Wilming, M. & Johnsson, K. (2001). Inter- and intramolecular domain interactions of the catalase-peroxidase KatG from *M. tuberculosis*. *FEBS Letters*, **509**, 272–276.
- Laskowski, R. A., MacArthur, M. W., Moss, D. S. & Thornton, J. M. (1993). PROCHECK: a program to check the stereochemical quality of protein structures. *J. Appl. Crystallog.* **26**, 283–291.
- Weik, M., Ravelli, R. B. G., Kryger, G., McSweeney, S., Raves, M. L., Harel, M. *et al.* (2000). Specific chemical and structural damage to proteins produced by synchrotron radiation. *Proc. Natl Acad. Sci USA*, **97**, 623–628.
- Ravelli, R. B. G. & McSweeney, S. M. (2000). The fingerprint that X-rays can leave on structures. *Structure*, **8**, 315–328.
- Chouchane, S., Lippai, I. & Magliozzo, R. S. (2000). Catalase-peroxidase (*Mycobacterium tuberculosis* KatG) catalysis and isoniazid activation. *Biochemistry*, **39**, 9975–9983.
- Creighton, T. E. (1993). *Proteins: Structures and Molecular Properties*, 2nd edit., Freeman, New York.
- Choinowski, T., Blodig, W., Winterhalter, K. H. & Piontek, K. (1999). The crystal structure of lignin peroxidase at 1.70 Å resolution reveals a hydroxy group on the C^β of tryptophan 171: a novel radical site formed during the redox cycle. *J. Mol. Biol.* **286**, 809–827.
- Henriksen, A., Welinder, K. G. & Gajhede, M. (1998). Structure of barley grain peroxidase refined at 1.9 Å resolution. *J. Biol. Chem.* **273**, 2241–2248.

21. Naruse, N., Oka, M., Konishi, M. & Oki, T. (1993). New antiviral antibiotics, kistamicins A and B. II. Structure determination. *J. Antibiot.* **46**, 1812–1818.
22. Elder, A. M. & Rich, D. H. (1999). Two syntheses of the 16- and 17-membered DEF ring systems of chloropeptin and complestatin. *Org. Letters*, **1**, 1443–1446.
23. Buzy, A., Bracchi, V., Sterjiades, R., Chroboczek, J., Thibault, P., Gagon, J. *et al.* (1995). Complete amino acid sequence of *Proteus mirabilis* PR catalase. Occurrence of a methionine sulfone in the close proximity of the active site. *J. Protein Chem.* **14**, 59–72.
24. Murshudov, G. N., Grebenko, A. I., Barynin, V., Dauter, Z., Wilson, K., Vainshtein, B. K. *et al.* (1996). Structure of the heme d of *Penicillium vitale* and *Escherichia coli* catalases. *J. Biol. Chem.* **271**, 8863–8868.
25. Bravo, J., Fita, I., Ferrer, J. C., Ens, W., Hillar, A., Switala, J. & Loewen, P. C. (1997). Identification of a novel bond between a histidine and the essential tyrosine in catalase HPII of *Escherichia coli*. *Protein Sci.* **6**, 1016–1023.
26. Henriksen, A., Schuller, D. J., Meno, K., Welinder, K. G., Smith, A. T. & Gajhede, M. (1998). Structural interactions between horseradish peroxidase C and the substrate benzhydroxamic acid determined by X-ray crystallography. *Biochemistry*, **37**, 8054–8060.
27. Rozawarski, D. A., Grant, G. A., Barton, D. H. R., Jacobs, W. R., Jr & Sacchettini, J. C. (1998). Modification of the NADH of the isoniazid target (INHA) from *Mycobacterium tuberculosis*. *Science*, **279**, 98–102.
28. Lei, B., Wei, C. J. & Tu, S. C. (2000). Activation mechanism of antitubercular isoniazid: activation by *Mycobacterium tuberculosis* KatG, isolation and characterization of InhA inhibitor. *J. Biol. Chem.* **275**, 2520–2526.
29. Rouse, D. A., DeVito, J. A., Li, Z., Byer, H. & Morris, S. L. (1996). Site-directed mutagenesis of the *katG* gene of *Mycobacterium tuberculosis*: effects on catalase-peroxidase activities and isoniazid resistance. *Mol. Microbiol.* **22**, 583–592.
30. Hillar, A. & Loewen, P. C. (1995). Comparison of isoniazid oxidation catalyzed by bacterial catalase-peroxidase and horseradish peroxidase. *Arch. Biochem. Biophys.* **323**, 438–446.
31. Otwinowski, Z. & Minor, W. (1996). Processing of X-ray diffraction data collected in oscillation mode. *Methods Enzymol.* **276**, 307–326.
32. Navaza, J. (1994). AMoRe: an automated package for molecular replacement. *Acta Crystallog. sect. A*, **50**, 157–163.
33. Lamzin, V. S. & Wilson, K. S. (1997). Automated refinement for protein crystallography. *Methods Enzymol.* **277**, 269–305.
34. Brünger, A. T., Adams, P. D., Clore, G. M., DeLano, W. L., Gros, P., Grosse-Kunstleve, R. W. *et al.* (1998). Crystallography and NMR system (CNS): a new software suite for macromolecular structure determination. *Acta Crystallog. sect. D*, **54**, 905–921.
35. Murshudov, G. N., Vagin, A. A. & Dodson, E. J. (1997). Refinement of macromolecular structures by the maximum-likelihood method. *Acta Crystallog. sect. D*, **53**, 240–255.
36. Collaborative Computational Project, Number 4 (1994). The CCP4 suite: programs for protein crystallography. *Acta Crystallog. sect. A*, **50**, 760–763.
37. Jones, T. A., Zou, J. Y., Cowan, S. W. & Kjeldgaard, M. (1991). Improved methods for building protein models in electron density maps. *Acta Crystallog. sect. A*, **47**, 110–119.
38. Kleywegt, G. J. & Jones, T. A. (1994). Detection, delineation, measurement and display of cavities in macromolecule structures. *Acta Crystallog. sect. D*, **50**, 178–185.
39. Maté, M. J., Sevinc, M. S., Hu, B., Bujons, J., Bravo, J., Switala, J. *et al.* (1999). Mutants that alter the covalent structure of catalase hydroperoxidase II from *Escherichia coli*. *J. Biol. Chem.* **274**, 27717–27725.
40. Evans, S. (1993). SETOR: hardware lighted three-dimensional solid model representations of macromolecules. *J. Mol. Graph.* **11**, 134–138.

Edited by R. Huber

(Received 24 October 2002; received in revised form 6 January 2003; accepted 17 January 2003)